

# A Numerical Study of Methods for Moist Atmospheric Flows: Compressible Equations

Max Duarte\*    Ann S. Almgren\*    Kaushik Balakrishnan\*    John B. Bell\*

David M. Romps<sup>†‡</sup>

September 1, 2019

## Abstract

We investigate different numerical techniques for integrating reversible moist processes in atmospheric flows in the context of solving the fully compressible Euler equations. We explore two common approaches: a one-step, coupled technique that relies on the use of conservative variables such as energy of moist air and total water content, and a two-step scheme that separately advances the dynamics and moist microphysics. The numerical techniques we describe are validated by comparing to a well-established benchmark problem. Particular attention is then paid to the effect of changing the time scale at which the moist variables are adjusted to the saturation requirements, as the use of a larger time step for saturation adjustment is common when acoustic modes are separately integrated in time, neglecting phase change related phenomena, or when evolving sound-proof equations. It is shown that incorporating the effects of reversible moist processes related to phase change on a slower time scale than the dynamics retains sufficient accuracy only as long as the moist thermodynamic properties are consistently updated and included while advancing the dynamics.

## 1 Introduction

Small-scale atmospheric phenomena are generally characterized by relatively slow dynamics, that is, low Mach number flows for which the fast acoustic modes are physically irrelevant. Historically, two main approaches have been used to overcome the computational restrictions resulting from resolving fast-propagating sound waves. The first and quite broad approach considers the fully compressible equations of motion (commonly referred to as elastic equations) with additional numerical treatments to limit the impact of acoustic modes, for instance, by advancing the acoustic signal in time with an implicit time discretization or with smaller time steps, as originally considered for cloud models in [28] and [15], among many other techniques. A second alternative consists of analytically filtering acoustic modes from the original compressible equations, thus deriving a new set of equations, often called sound-proof equations. Within this category are anelastic models [2, 19, 8, 10] and pseudo-incompressible formulations [6], both of which have been extended to moist atmospheres, e.g., in [4, 18] and [20]. A comparison of moist simulations performed with two different anelastic models and a fully compressible model was recently presented by [17].

In many cases atmospheric flow models, based on either compressible or sound-proof equations, are recast in terms of the potential temperature as the main thermodynamic variable, a choice motivated by the fact that potential temperature is an invariant of adiabatic processes for dry air. Additionally, the Exner function is commonly used to define a dimensionless pressure. Extending

---

\*Center for Computational Sciences and Engineering, Lawrence Berkeley National Laboratory, Berkeley, CA 94720

<sup>†</sup>Dept. of Earth and Planetary Science, University of California, Berkeley, Berkeley, CA 94720

<sup>‡</sup>Earth Sciences Division, Lawrence Berkeley National Laboratory, Berkeley, CA 94720

this formalism to moist atmospheres constitutes a widely accepted practice, which usually involves a definition of equivalent potential temperature (e.g., [15]). Alternatively, [21] proposed a return to the primitive equations of motion in which prognostic equations for the dynamics are formulated in terms of conservative variables, while other thermodynamic variables, including pressure, are recovered diagnostically. This formulation was later extended to include irreversible thermodynamic processes (like precipitation) in [22], and inspired the development of some other conservative schemes considering both primitive variables (e.g., [24, 25, 26]) and an equivalent potential temperature formalism (e.g., [16]).

Whether an elastic or a sound-proof formulation is adopted, and regardless of the choice of variables, a key question in moist atmospheric flow modeling involves the treatment of reversible and irreversible moist mechanisms. In this paper we investigate the interplay between the dynamics and the thermodynamics of reversible process, i.e., water phase changes, using an exact Clausius-Clapeyron formula for moist thermodynamics and considering the effects of the specific heats of water and the temperature dependency of the latent heat (as in [25, 23]). Specifically, we want to characterize the impact of modifying the time scale at which the moist thermodynamics is adjusted to the saturation requirements.

For this purpose, we follow the approach of [21] in formulating the problem based on the separation of dynamics and thermodynamics, and explicitly evolve the compressible Euler equations at the acoustic time scale, allowing us to focus on issues of how to consistently couple the moist thermodynamic processes to the dynamics without regard to issues associated with evolving the dynamics at different time scales. In the same spirit, we write the Euler equations in conservation law form (similar to [25]), which eases the inclusion of time-varying thermodynamic parameters for moist air. Further discussion of more efficient procedures to solve the dynamics, i.e. methods that do not explicitly resolve the fast acoustic modes, is orthogonal to the current study and is out of the scope of the present work.

With this formulation, we consider two classical ways to numerically handle moist microphysics (see, e.g., [12]). The first and more common approach considers a two-step technique that first solves the equations of dry dynamics, and then applies an adjustment step that takes into account phase changes (cf. [27]). (This is the case, for instance, in [15, 25].) In the second approach, often referred to as the invariant (conservative) variables approach, the equations of motion are solved by defining appropriate invariant variables such that terms resulting from phase change are eliminated in the governing equations, while the remaining variables are diagnostically recovered (cf. [14]). (This is the case, for instance, in [21, 22] for total water content and entropy.)

## 2 Governing equations

We begin by writing the fully compressible equations of motion expressing conservation of mass, momentum, and energy (taken as internal plus kinetic energies), in a constant gravitational field,

$$\frac{\partial \rho}{\partial t} + \nabla \cdot (\rho \mathbf{u}) = 0, \quad (1)$$

$$\frac{\partial (\rho \mathbf{u})}{\partial t} + \nabla \cdot (\rho \mathbf{u} \mathbf{u}) + \nabla p = -\rho g \hat{\mathbf{e}}_z, \quad (2)$$

$$\frac{\partial (\rho E)}{\partial t} + \nabla \cdot (\rho E \mathbf{u} + p \mathbf{u}) = -\rho g (\mathbf{u} \cdot \hat{\mathbf{e}}_z), \quad (3)$$

in which we neglect Coriolis forces and viscous terms, as well as the influence of thermal conduction and radiation. Here  $\rho$  and  $\mathbf{u}$  are the density and velocity, respectively; the energy,  $E$ , is defined as the sum of internal plus kinetic energies, and the pressure,  $p$ , is defined by an equation of state (EOS). We include gravitational acceleration given by  $\mathbf{g} = -g \hat{\mathbf{e}}_z$ , where  $\hat{\mathbf{e}}_z$  is the unit vector in the vertical direction.

We then follow the formalism as in [23] for moist atmospheres with the additional simplification that all phases have the same temperature and velocity field. Here we also ignore ice-phase microphysics, precipitation fallout, and subgrid-scale turbulence. Considering an atmosphere with three components: dry air, water vapor, and liquid water; moist air is treated as an ideal mixture with water phases in thermodynamic equilibrium, so that only reversible processes are taken into account. Denoting by  $q_a$ ,  $q_v$ , and  $q_l$  the mass fraction of dry air, water vapor, and liquid water, respectively, we can also express the conservation of mass (1) in terms of the following equations:

$$\frac{\partial(\rho q_a)}{\partial t} + \nabla \cdot (\rho q_a \mathbf{u}) = 0, \quad (4)$$

$$\frac{\partial(\rho q_v)}{\partial t} + \nabla \cdot (\rho q_v \mathbf{u}) = e_v, \quad (5)$$

$$\frac{\partial(\rho q_l)}{\partial t} + \nabla \cdot (\rho q_l \mathbf{u}) = -e_v, \quad (6)$$

noting that  $q_a + q_v + q_l = 1$  with  $\rho$  being the density of moist air. The evaporation rate,  $e_v$ , has dimensions of mass per volume per time; negative values of  $e_v$  correspond to condensation. Introducing the mass fraction of total water,  $q_w = q_v + q_l$ , equations (5)–(6) can be also recast as

$$\frac{\partial(\rho q_w)}{\partial t} + \nabla \cdot (\rho q_w \mathbf{u}) = 0. \quad (7)$$

The energy  $E$  in (3) is defined in this work as

$$E = \hat{e} + \frac{\mathbf{u} \cdot \mathbf{u}}{2},$$

where  $\hat{e}$  stands for the specific internal energy of moist air. The constant-volume specific heat of moist air is given by

$$c_{vm} = q_a c_{va} + q_v c_{vv} + q_l c_{vl},$$

with constant specific heats at constant volume:  $c_{va}$ ,  $c_{vv}$ , and  $c_{vl}$ , for the three components: air, water vapor, and liquid water, respectively. The internal energy of moist air is thus defined as

$$\hat{e} = c_{vm} (T - T_{\text{trip}}) + q_v e_{0v}, \quad (8)$$

where  $T_{\text{trip}}$  is the triple-point temperature, and  $e_{0v}$  is the specific internal energy of water vapor at the triple point. [25] considered also the same formulation, in particular for the internal energy of moist air (8), but total energy (internal plus kinetic plus potential energies) is considered instead of  $E$ .

An equation of state for moist air must be provided to close the system. For the sake of illustration, we consider in this study a standard approach adopted in atmospheric flows in which dry air and water vapor are treated as ideal gases (see, e.g., [21, 25, 16]). The partial pressures of dry air and water vapor are then given by

$$p_a = \rho q_a R_a T, \quad (9)$$

$$p_v = \rho q_v R_v T, \quad (10)$$

where  $R_a$  and  $R_v$  are the specific gas constants for dry air and water vapor, respectively. Denoting by  $M_a$  and  $M_v$  the molar masses of dry air and water, respectively, we know that  $R_a = R/M_a$  and  $R_v = R/M_v$ , where  $R$  is the universal gas constant for ideal gases. The sum of the partial pressures, (9) and (10), defines the total pressure of a parcel,

$$p = p_a + p_v = \rho R_m T, \quad (11)$$

thus defining the specific gas constant of moist air,

$$R_m = q_a R_a + q_v R_v = \left( \frac{q_a}{M_a} + \frac{q_v}{M_v} \right) R .$$

Additionally, the specific heat capacities at constant pressure can be defined as

$$c_{pa} = c_{va} + R_a, \quad c_{pv} = c_{vv} + R_v, \quad c_{pm} = c_{vm} + R_m,$$

for dry air, water vapor, and moist air, respectively. Notice that here we include specific heats for all three phases; by contrast, a standard approximation in cloud models consists of neglecting the specific heats of water vapor and liquid water.

Now, the saturation vapor pressure with respect to liquid water,  $p_v^*$ , is defined by the following Clausius-Clapeyron relation:

$$p_v^*(T) = p_{\text{trip}} \left( \frac{T}{T_{\text{trip}}} \right)^{\alpha_v} \exp \left[ \beta_v \left( \frac{1}{T_{\text{trip}}} - \frac{1}{T} \right) \right], \quad (12)$$

with constants  $\alpha_v$  and  $\beta_v$ , given, for instance, by

$$\alpha_v = \frac{c_{pv} - c_{vl}}{R_v}, \quad \beta_v = \frac{e_{0v} - (c_{vv} - c_{vl})T_{\text{trip}}}{R_v}, \quad (13)$$

according to [23]. The saturated mass fraction of water vapor,  $q_v^*$ , can be then computed based on the EOS, given in this case by

$$q_v^*(\rho, T) = \frac{p_v^*}{\rho R_v T}, \quad (14)$$

following (10). Following [21, 25], we assume that air parcels cannot be supersaturated, and thus water vapor mass fraction,  $q_v$ , cannot exceed its saturated value:  $q_v^*$ .

### 3 Numerical Methodology

In what follows we describe the numerical methodology we use to solve the compressible equations (1)–(6) for moist flows. The detailed numerics for dry flow are as described in [1], which describes the CASTRO code, a multicomponent compressible solver designed to model astrophysical flows. Our attention here will be mainly focused on the incorporation of moist reversible processes. We distinguish two approaches depending on the way thermodynamics and, in particular, phase transitions are handled within the numerical solution of the overall flow dynamics (see, e.g., [12]). We will refer to the first case as the one-step coupled scheme where the derived formulation without source terms related to phase changes allows a standard numerical resolution of the dynamics (as in the dry case), while thermodynamic variables (especially pressure) are recovered by diagnostic relationships according to moist microphysics and the saturation requirements. The second technique, denoted as the two-step split scheme, involves the numerical solution of the dynamics neglecting phase change related terms, followed by an adjustment step that impose the saturation requirements of the final solution for temperature and moisture variables [27]. Our formulation and implementation of moist microphysics for the first and second configurations are similar, respectively, to [21] and [25].

### 3.1 One-step Coupled Scheme

We consider the following set of evolution equations:

$$\left. \begin{aligned} \frac{\partial \rho}{\partial t} + \nabla \cdot (\rho \mathbf{u}) &= 0, \\ \frac{\partial (\rho \mathbf{u})}{\partial t} + \nabla \cdot (\rho \mathbf{u} \mathbf{u}) + \nabla p &= -\rho g \hat{\mathbf{e}}_z, \\ \frac{\partial (\rho E)}{\partial t} + \nabla \cdot (\rho E \mathbf{u} + p \mathbf{u}) &= -\rho g (\mathbf{u} \cdot \hat{\mathbf{e}}_z), \\ \frac{\partial (\rho q_a)}{\partial t} + \nabla \cdot (\rho q_a \mathbf{u}) &= 0, \\ \frac{\partial (\rho q_w)}{\partial t} + \nabla \cdot (\rho q_w \mathbf{u}) &= 0, \end{aligned} \right\} \quad (15)$$

for  $(\rho, \mathbf{u}, E, q_a, q_w, p)$ , and close the system with the moist EOS (11). [21] considers the same formulation but the conservation equation for entropy density of moist air is considered instead of  $(\rho E)$ . We refer to  $\mathbf{U} = (\rho, \rho \mathbf{u}, \rho E, \rho q_a, \rho q_w)$  as the conserved variables, and the time evolution of  $\mathbf{U}$  can be written in the form

$$\frac{\partial \mathbf{U}}{\partial t} = -\nabla \cdot \mathbf{F} + \mathbf{S}_g,$$

using a finite volume discretization, where  $\mathbf{F}$  is the flux vector and  $\mathbf{S}_g$  represents only the gravitational source terms in the equations for momentum and energy. We advance the solution  $\mathbf{U}$  by one time step  $\Delta t$  using the time discretization,

$$\mathbf{U}^{n+1} = \mathbf{U}^n - \Delta t \nabla \cdot \mathbf{F}^{n+1/2} + \Delta t \mathbf{S}_g^{n+1/2}. \quad (16)$$

The construction of  $\mathbf{F}$  is purely explicit, and based on an unsplit Godunov method with characteristic tracing. The solution  $\mathbf{U}$  is defined on cell centers; we predict the primitive variables,  $\mathbf{Q} = (\rho, \mathbf{u}, p, \rho \hat{e}, q_a, q_w)$ , from cell centers at time  $t^n$  to edges at time  $t^{n+1/2}$ , and use an approximate Riemann solver to construct fluxes  $\mathbf{F}^{n+1/2}$  on cell faces. We refer to [1] for complete details on this numerical implementation. This algorithm is formally second-order in both space and time.

System (15) is advanced in time without neglecting any terms, and considering consistent moist thermodynamics through the pressure terms derived from the moist equation of state as shown below. This approach is coupled in the sense that the moist processes are incorporated as part of the dynamical evolution of the system. Given  $(\rho, \mathbf{u}, E, q_a, q_w)$ , using the Clausius-Clapeyron relation and the saturation requirements, the values of  $(q_v, q_l, T)$  can be obtained by solving the following nonlinear system of equations [25]:

$$\left. \begin{aligned} \hat{e} &= E - \frac{\mathbf{u} \cdot \mathbf{u}}{2} = c_{vm}(q_a, q_v, q_l) (T - T_{\text{trip}}) + q_v e_{0v}, \\ q_v &= \min [q_v^*(\rho, T), q_w], \\ q_l &= q_w - q_v. \end{aligned} \right\} \quad (17)$$

The pressure  $p$ , needed to close system (15), is hence computed from the moist EOS (11) with the known  $(q_v, q_l, T)$ , solutions of (17). System (17) is numerically solved in each cell to determine the local temperature  $T$ , as well as the water mass fractions  $q_v$  and  $q_l$ , by considering an iterative Newton solver, detailed in the following for the sake of completeness:

**Step 1: Initialization.** Define initial guess:  $\tilde{T} = T_{\text{old}}$ , where  $T_{\text{old}}$  is the last known temperature at the current cell.

**Step 2: Compute mass fractions:**  $q_v$  and  $q_l$ . Following the Clausius-Clapeyron relation (12), compute

$$\tilde{p}_v^*(\tilde{T}) = p_{\text{trip}} \left( \frac{\tilde{T}}{T_{\text{trip}}} \right)^{\alpha_v} \exp \left[ \beta_v \left( \frac{1}{T_{\text{trip}}} - \frac{1}{\tilde{T}} \right) \right],$$

and  $\tilde{q}_v^* = \tilde{q}_v^*(\rho, \tilde{T})$  from (14), so that

$$\tilde{q}_v = \min[\tilde{q}_v^*, q_w], \quad \tilde{q}_l = q_w - \tilde{q}_v,$$

and we can evaluate

$$\tilde{e} = c_{vm}(q_a, \tilde{q}_v, \tilde{q}_l) (\tilde{T} - T_{\text{trip}}) + \tilde{q}_v e_{0v}.$$

**Step 3:** *Update temperature: T.* Define a local function:  $f(\tilde{T}) = \tilde{e} - \hat{e}$ , and update  $\tilde{T}$  by computing a Newton correction step:

$$\tilde{T} = \tilde{T} - \Delta\tilde{T}, \quad \Delta\tilde{T} = f(\tilde{T})/\partial_{\tilde{T}}f(\tilde{T}),$$

where

$$\partial_{\tilde{T}}f = \partial_{\tilde{T}}q_v^*(L_e - R_vT) + c_{vm}, \quad \partial_{\tilde{T}}q_v^* = q_v^* \left( \frac{\alpha_v - 1}{\tilde{T}} + \frac{\beta_v}{\tilde{T}^2} \right),$$

with the latent heat of vaporization,  $L_e$ , defined as

$$L_e = e_{0v} + R_vT + (c_{vv} - c_{vl})(T - T_{\text{trip}}). \quad (18)$$

**Step 4:** *Stopping criterion.* Introducing an accuracy tolerance,  $tol$ , and denoting  $err = |\Delta\tilde{T}/\tilde{T}|$ , we define the following stopping criterion:

- If  $err > tol$ : go back to **Step 2**;
- If  $err \leq tol$ : stop iterating and set  $T = \tilde{T}$ ,  $q_v = \tilde{q}_v$ , and  $q_l = \tilde{q}_l$ .

Notice that if  $q_w < q_v^*$ , all water is in the form of vapor, that is,  $q_v = q_w$  and  $q_l = 0$ ; the temperature is hence directly computed from (8), or equivalently from **Steps 1-4** considering that in this case:  $\partial_{\tilde{T}}f = c_{vm}$ . This procedure remains valid for any moist equation of state, as long as a Clausius-Clapeyron relation (12) is available to define the saturation pressure.

The time step in (16) is computed using the standard CFL condition for explicit methods. Following [1], we set a CFL factor  $\sigma^{\text{CFL}}$  between 0 and 1, and for a calculation in  $n_{\text{dim}}$  dimensions,

$$\Delta t = \sigma^{\text{CFL}} \min_{i=1 \dots n_{\text{dim}}} \{\Delta t_i\}, \quad \Delta t_i = \frac{\Delta x_i}{|\mathbf{u}_i| + c_m}, \quad (19)$$

with  $c_m$ , the sound speed in moist air, and  $\Delta t_i$  computed as the minimum over all cells. The sound speed is computed using the moist EOS, and it is defined in this study as for an ideal gas:

$$c_m = \sqrt{\gamma_m \frac{p}{\rho}}, \quad \gamma_m = \frac{c_{pm}^g}{c_{vm}^g},$$

where  $\gamma_m$  is the isentropic expansion factor of moist air, computed based only on the gaseous components:

$$c_{vm}^g = q_a c_{va} + q_v c_{vv}, \quad c_{pm}^g = c_{vm}^g + R_m.$$

## 3.2 Two-step Split Scheme

In this case we consider the following set of equations for the dynamics:

$$\left. \begin{aligned} \frac{\partial \rho}{\partial t} + \nabla \cdot (\rho \mathbf{u}) &= 0, \\ \frac{\partial (\rho \mathbf{u})}{\partial t} + \nabla \cdot (\rho \mathbf{u} \mathbf{u}) + \nabla p &= -\rho g \hat{\mathbf{e}}_z, \\ \frac{\partial (\rho E)}{\partial t} + \nabla \cdot (\rho E \mathbf{u} + p \mathbf{u}) &= -\rho g (\mathbf{u} \cdot \hat{\mathbf{e}}_z), \\ \frac{\partial (\rho q_a)}{\partial t} + \nabla \cdot (\rho q_a \mathbf{u}) &= 0, \\ \frac{\partial (\rho q_v)}{\partial t} + \nabla \cdot (\rho q_v \mathbf{u}) &= 0, \\ \frac{\partial (\rho q_l)}{\partial t} + \nabla \cdot (\rho q_l \mathbf{u}) &= 0, \end{aligned} \right\} \quad (20)$$

where terms related to phase change are set to zero, that is,  $e_v = 0$  in (5) and (6). [25] considers the same setup but an equation for internal energy accounting only for sensible heat is used instead of  $(\rho E)$ . A source term corresponding to the latent heat release appears then in the conservation equation for energy, contrary to our formulation. In our case only equations for  $q_v$  and  $q_l$  explicitly contain information on the water phase transitions, which eases the implementation of both the one- and two-step schemes for the purposes of the present study.

In this scheme to account for saturation requirements and phase change, a separate procedure is performed to correct moist variables and temperature (and hence pressure) in the solutions obtained after advancing the dynamics. Defining  $t_{\text{sat}}$  and  $\Delta t_{\text{sat}}$  as, respectively, the time and the time interval for this adjustment step, we can schematically describe the method as a two-step procedure:

**Step A:** *Advance dynamics through  $\Delta t$ .* Advance (20) in time from  $t$  to  $t + \Delta t$ , solving for the conserved variables:  $\mathbf{U} = (\rho, \rho \mathbf{u}, \rho E, \rho q_a, \rho q_v, \rho q_l)$ . With  $(q_a, q_v, q_l, \hat{\mathbf{e}})$ , temperature is computed from (8), and therefore pressure from the EOS (11) to close system (20).

**Step B:** *Moist microphysics adjustment.* This step is performed only if  $t \geq t_{\text{sat}} + \Delta t_{\text{sat}}$ , where  $t_{\text{sat}}$  records the last time the correction step was computed, and  $\Delta t_{\text{sat}}$  is a pre-specified interval. Thus, if  $t \geq t_{\text{sat}} + \Delta t_{\text{sat}}$ : solve (17) for  $T$ ,  $q_v$ , and  $q_l$ , given  $(\rho, \hat{\mathbf{e}}, q_a, q_w = q_v + q_l)$ , using the iterative procedure described in **Steps 1-4**. Pressure is also corrected once we have the adjusted temperature and moist variables. Set  $t_{\text{sat}} = t$ .

Notice that  $\Delta t_{\text{sat}} = 0$ , involves correcting moist and thermodynamic variables after each time integration step  $\Delta t$  of the dynamics. With respect to the incorporation of moist processes, this two-step procedure is equivalent to a splitting approach in which dynamics and moist thermodynamics related to phase changes are separately considered. In particular the larger  $\Delta t_{\text{sat}}$  is, the more the dynamics evolve neglecting phase changes. Recall that our numerical implementation does not discriminate between fast and slow modes associated with the compressible equations; therefore, **Step B** with  $\Delta t_{\text{sat}} > \Delta t$ , where  $\Delta t$  is limited by the acoustics, necessarily involves several dynamical time steps  $\Delta t$  before a saturation adjustment is performed.

However, one alternative to this method consists in partially accounting for moist processes consistent with the saturation requirements during the numerical integration of the dynamics. The latter is achieved with our formulation by computing the pressure with adjusted values of moist variables and temperature. In this case **Step A** will now read as

**Step A\*:** *Advance dynamics through  $\Delta t$ .* Advance (20) in time from  $t$  to  $t + \Delta t$ , solving for the conserved variables:  $\mathbf{U} = (\rho, \rho \mathbf{u}, \rho E, \rho q_a, \rho q_v, \rho q_l)$ . Pressure is defined by the EOS (11) with moist variables and temperature obtained through the iterative procedure **Steps 1-4** to solve (17) such that saturation requirements are satisfied.

Notice however that **Step A\*** still neglects the source terms involving phase change in (20) during integration. Therefore the moist variables,  $q_v$  and  $q_l$ , obtained after numerical integration do not necessarily satisfy the saturation requirements unless there is no phase transition during  $\Delta t$ . **Step B** is hence still required.

Other attempts to improve the quality of the two-step approximation consider, for instance, solving the dynamics with all terms involving phase change, which are either estimated or predicted based on the available information such as the solution corresponding to the previous time step. A second step like **Step B** is then performed to adjust temperature and moist variables. This is the case, for instance, in [13] and [16], where a different formulation based on potential temperature is considered, and thus phase change related terms appear in the equations for moist variables and potential temperature.

## 4 Numerical Simulations

In what follows we first consider the benchmark simulations proposed in [3] for moist flows, along with the corresponding configuration for dry air originally presented in [29]. Both cases are presented and results are compared with those obtained in [3] in order to first validate our numerical implementation. We then compare the approximations obtained with the different numerical schemes previously described. In particular, we investigate the impact of the time interval of saturation adjustment  $\Delta t_{\text{sat}}$  on the moist flow. A second configuration based on [5, 11] is also studied for non-isentropic background states and both saturated and only partially saturated media, to further assess the different numerical techniques.

### 4.1 Benchmark Simulations

[3] present solutions of a benchmark test case using the fully compressible equations, where the conservation equations for vapor and liquid water are written in terms of the water vapor and cloud mixing ratios:  $r_v = q_v/q_a$  and  $r_c = q_l/q_a$ , respectively. The conservation equation for energy (3) is replaced by

$$\rho c_{vm} \left( \frac{\partial T}{\partial t} + \mathbf{u} \cdot \nabla T \right) = -p (\nabla \cdot \mathbf{u}) - (L_v - R_v T) e_v,$$

with the latent heat of vaporization  $L_v$  defined as

$$L_v = L_{v0} - (c_{pl} - c_{pv})(T - T_0), \quad (21)$$

where  $L_{v0}$  and  $T_0$  are constant reference values of  $L_v$  and temperature, respectively. A nondimensional Exner pressure  $\pi$  and the potential temperature  $\theta$  are considered in [3], defined as

$$\pi = \left( \frac{p}{p_{00}} \right)^{R_a/c_{pa}}, \quad \theta = \frac{T}{\pi}, \quad (22)$$

where  $p_{00} = 1000$  mb. The numerical scheme thus solves time dependent equations for  $(\mathbf{u}, \pi, \theta, r_v, r_c)$ , where the evaporation rate  $e_v$  appears in the source terms for the equations for  $\pi$ ,  $\theta$ ,  $r_v$ , and  $r_c$ . The technique introduced in [15] is considered to integrate the equations in two steps: a dynamical step and the microphysics step. In the dynamical step, dynamics is solved neglecting  $e_v$ ; portions of the governing equations that support acoustic waves are updated on a smaller time step than other terms. The model is integrated with a third order Runge-Kutta scheme and fifth order spatial discretization for the advective terms. Then, a saturation adjustment technique, similar to that proposed by [27], is considered in the microphysics step in which only the terms involving phase change are included. Notice that this approach is similar to our **A-B** procedure described in §33.2, with the main difference that phase change related terms appear only in the equations for water variables,  $q_v$  and  $q_l$ , in our formulation.

The hydrostatic base state pressure can be found through

$$\frac{d\pi_0}{dz} = -\frac{g}{c_{pa}\theta_{\rho 0}}, \quad (23)$$

where subscript 0 stands for hydrostatic base quantities, and the density potential temperature  $\theta_\rho$  is defined as

$$\theta_\rho = \theta \frac{(1 + r_v/\epsilon)}{(1 + r_t)}, \quad (24)$$

with the total water mixing ratio:  $r_t = q_w/q_a$ .

For the next computations we consider the following constant parameters, taken from [3]:  $R_a = 287 \text{ J kg}^{-1} \text{ K}^{-1}$ ,  $R_v = 461 \text{ J kg}^{-1} \text{ K}^{-1}$ ,  $L_{v0} = 2.5 \times 10^6 \text{ J kg}^{-1}$ ,  $c_{va} = 717 \text{ J kg}^{-1} \text{ K}^{-1}$ ,  $c_{vv} = 1424 \text{ J kg}^{-1} \text{ K}^{-1}$ ,  $c_{pl} = 4186 \text{ J kg}^{-1} \text{ K}^{-1}$ ,  $T_0 = 273.15 \text{ K}$ , and  $g = 9.81 \text{ m s}^{-1}$ . The remaining parameters used in our model are defined such that we have the same definition of the latent heat of vaporization, that is,  $L_v = L_e$  from (21) and (18). Therefore we just need to consider:  $T_{\text{trip}} = T_0$ ,  $c_{vl} = c_{pl}$ , and  $e_{0v} = L_{v0} - R_v T_{\text{trip}}$ . The saturation vapor pressure is computed with the Clausius–Clapeyron equation (12) with constants:  $\alpha_v = 0$  and  $\beta_v = L_{v0}/R_v$ , with  $p_{\text{trip}} = 611 \text{ Pa}$ , taken from [20] that considers also the same benchmark problem.

#### 4.1.1 The Dry Simulation

Following [29] and [3], we consider a two-dimensional computational domain with height 10 km and width 20 km. The initial atmospheric environment is defined by a constant potential temperature of  $\theta_0 = 300 \text{ K}$ , and the pressure field is obtained by integrating upwards the hydrostatic equation (23). A warm perturbation is introduced in the domain, given by

$$\theta' = 2 \cos^2 \left( \frac{\pi L}{2} \right), \quad (25)$$

where

$$L = \min \left\{ 1, \sqrt{\left( \frac{x - x_c}{x_r} \right)^2 + \left( \frac{z - z_c}{z_r} \right)^2} \right\}, \quad (26)$$

with  $x_c = 10 \text{ km}$ ,  $z_c = 2 \text{ km}$ , and  $x_r = z_r = 2 \text{ km}$ . Notice that our formulation does not use the  $\theta - \pi$  formalism; the expressions (22) are used for the conversions, while the initial perturbation (25) is applied at constant pressure  $p(z)$ . We impose zero normal velocities and homogeneous Neumann boundary conditions for the tangential velocity components on all four boundaries. For the thermodynamic variables, homogeneous Neumann boundary conditions are considered at the horizontal sides, whereas the background state is reconstructed by extrapolation outside vertical boundaries in order to determine the corresponding fluxes.

Let us first consider a uniform grid of  $256 \times 128$  points, slightly finer than the original 100 m grid spacing in [3]. For all computations the CFL factor is given by:  $\sigma^{\text{CFL}} = 0.9$  in (19). The latter yields time steps roughly constant of about 0.2s in this configuration for the dry thermal computations. Figure 1 (left) illustrates the numerical results for the perturbation potential temperature ( $\theta' = \theta - \theta_0$ ) after 1000 s. The maximum and minimum values for  $\theta'$  are given by 2.09923 and  $-0.18525$ , respectively, compared with the original 2.07178 and  $-0.144409$  in [3]. Very good resemblance is in general found with respect to the reference solutions, also in terms of the height and width of the rising thermal. However, some differences in the dynamics can be appreciated around the two vortices developed on the sides of the thermal. In [3] both tips of the thermal seem to roll up slightly higher around the vortex cores. The maximum and minimum values of vertical velocity are in fact localized in this region, which in our computation are given by  $12.4991 \text{ m s}^{-1}$  and  $-7.58896 \text{ m s}^{-1}$ , respectively, slightly lower than  $14.5396 \text{ m s}^{-1}$  and  $-8.58069 \text{ m s}^{-1}$  in [3].

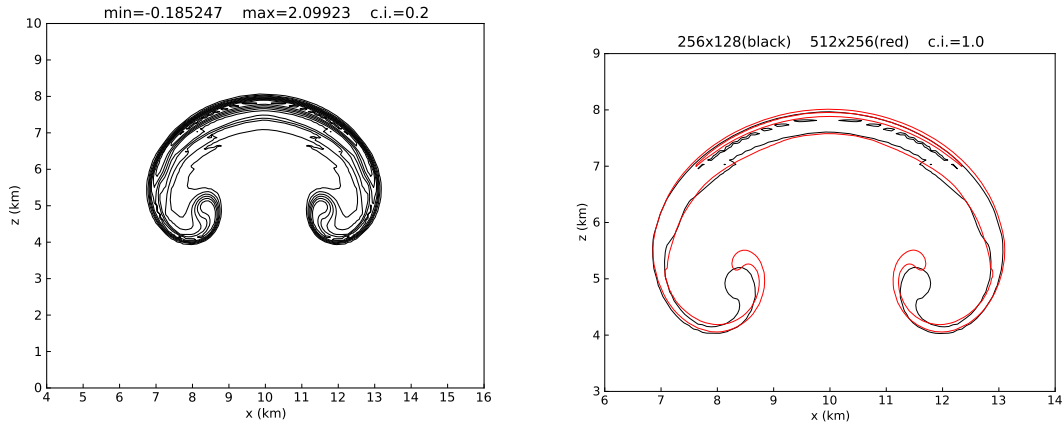


Figure 1: Dry thermal simulation at 1000 s. Left: perturbation potential temperature on a  $256 \times 128$  grid, contoured every 0.2 K. Right: comparison of the perturbation potential temperature computed on a  $256 \times 128$  (black) and  $512 \times 256$  (red) grids, contours every 1 K.

Besides the different choice of variables, there are two main differences between our implementation and the one in [3] that may explain the height difference of the thermal tips. The first difference concerns the higher order discretization in both time and space considered in [3]. The second one is given by the numerical decoupling of acoustic waves considered in [3]. Figure 1 (right) shows the same results for  $\theta'$  and a  $256 \times 128$  grid, compared with a solution computed using the same numerical scheme this time on a finer grid of  $512 \times 256$  (consequently, time steps are roughly halved to 0.1 s). It can be thus seen that a higher spatial resolution compensates for the lower order spatial discretization and yields better agreement with the benchmark solution in [3], as seen in Figure 2. In particular, maximum and minimum values of vertical velocity are this time equal to  $13.9372 \text{ m s}^{-1}$  and  $-8.30085 \text{ m s}^{-1}$ , respectively.

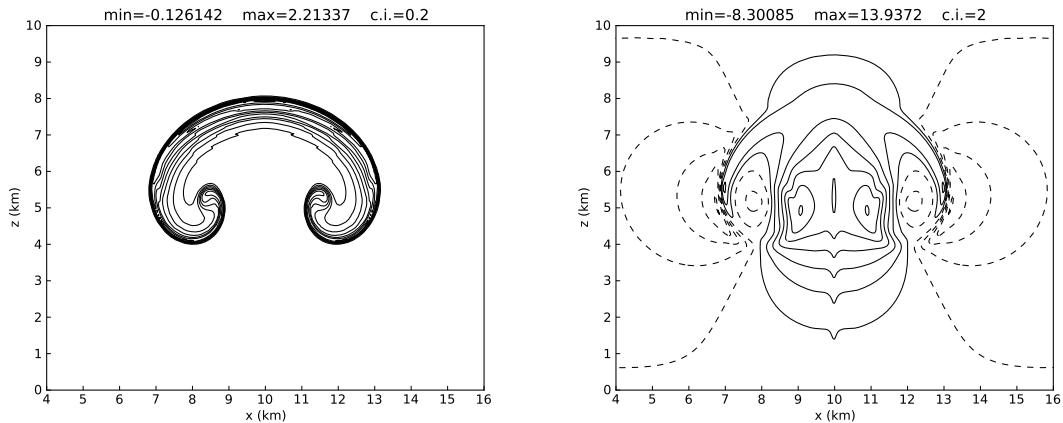


Figure 2: Dry thermal simulation at 1000 s on a  $512 \times 256$  grid. Left: perturbation potential temperature contoured every 0.2 K. Right: vertical velocity contoured every  $2 \text{ m s}^{-1}$ , negative contours are dashed. Contrast to Fig. 1 in [3].

### 4.1.2 The Moist Simulation

Here we consider the same configuration as above, but now with a moist atmospheric environment. A neutrally stable environment can be obtained by considering the wet equivalent potential temperature  $\theta_e$ , defined for a reversible moist adiabatic atmosphere by

$$\theta_e = T \left( \frac{p_a}{p_{00}} \right)^{-R_a/(c_{pa}+c_{pl}r_t)} \exp \left[ \frac{L_v r_v}{(c_{pa} + c_{pl}r_t)T} \right], \quad (27)$$

taken from [9]. Supposing that the total water mixing ratio is constant at all levels, the vertical profiles of  $\pi$ ,  $\theta$ ,  $r_v$ , and  $r_c$  can be obtained using (23), (24), and (27), if values for  $\theta_e$  and  $r_t$  are provided. We finally compute the hydrostatic base state written in terms of  $p$ ,  $T$ ,  $q_v$ , and  $q_l$  in our formulation. The value of  $r_t$  must be greater than  $r_{vs} = q_v^*/q_a$ , so that the initial environment is saturated, that is,  $q_v = q_v^*$  and  $q_l > 0$  everywhere in the domain. The initial perturbation (25) is then introduced in such a way that the buoyancy fields are identical in both the dry and moist simulations, when  $\theta_0 = 300$  K in the dry case [3]. The initial field for  $\theta$  is thus given by

$$\theta(p, T) \left( 1 + \frac{r_{vs}(p, T)}{\epsilon} \right) = \theta_{\rho 0} (1 + r_t) \left( \frac{\theta'}{300} + 1 \right),$$

with  $\epsilon = R_a/R_v = M_v/M_a$ , which is solved for  $T$ , point-wise throughout the domain at constant pressure  $p(z)$ .

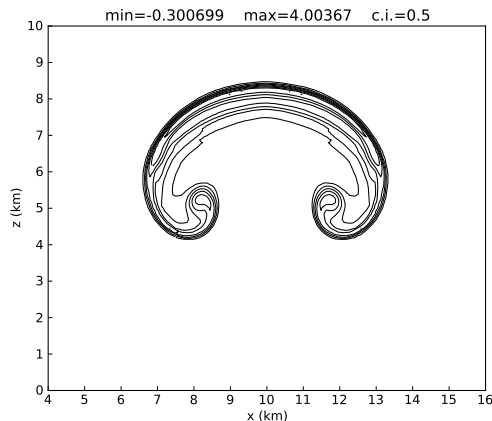


Figure 3: Moist thermal simulation at 1000 s. Perturbation potential temperature on a  $256 \times 128$  grid, contoured every 0.5 K.

Let us consider the one-step coupled scheme described in section 33.1 to compute the moist rising thermal with input parameters:  $\theta_{e0} = 320$  K and  $r_t = 0.02$ . For a  $256 \times 128$  grid, time steps are roughly constant of about 0.21 s, similar to the dry computation. The introduction of moist microphysics involves an additional cost of approximately 15 to 20% in CPU time with respect to the dry computation, which roughly corresponds to the computational cost of the Newton iterative procedure, described through **Steps 1-4** in section 33.1, to solve the nonlinear system (17) throughout the domain. (A fixed tolerance  $tol = 10^{-10}$  have been considered in this paper for the Newton solver.) The maximum and minimum values for the perturbation wet equivalent potential temperature ( $\theta'_e = \theta_e - \theta_{e0}$ ) are given by 4.00367 and  $-0.300699$ , respectively, compared with the original 4.09521 and  $-0.305695$  in [3]. Our computation yields  $13.3267 \text{ m s}^{-1}$  and  $-8.77365 \text{ m s}^{-1}$ , for the maximum and minimum vertical velocities, respectively, which are slightly lower than

15.7130 m s<sup>-1</sup> and -9.92698 m s<sup>-1</sup> in [3]. The solutions are practically identical in terms of position, height, and width of the thermal, as seen in Figure 3. Some differences can nevertheless be observed around the vortex cores, as in the previous dry computation. An additional difference between both implementations is that in our case moist microphysics and saturation requirements are considered coupled with the dynamics through the equation of state. Increasing the space resolution as before yields even better agreement, as seen in Figure 4 for a 512 × 256 grid. For instance, the maximum and minimum values of vertical velocity are now 15.3301 m s<sup>-1</sup> and -9.68717 m s<sup>-1</sup>, respectively.

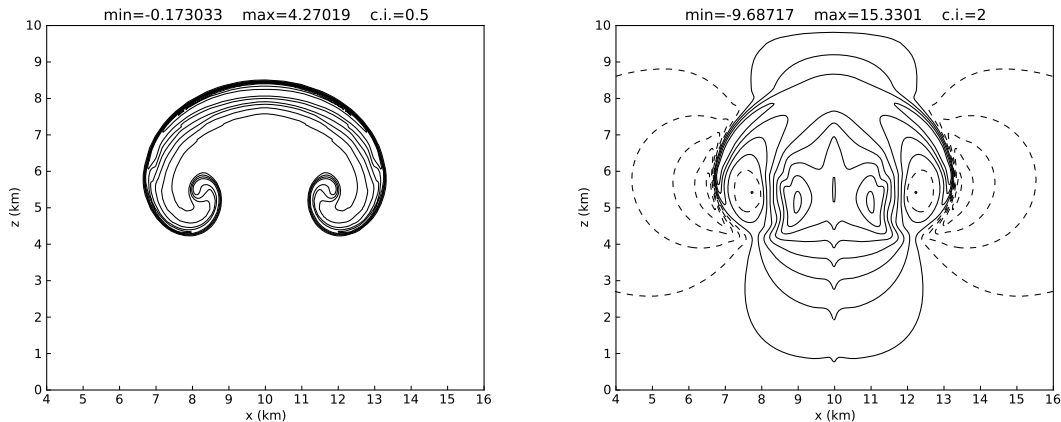


Figure 4: Moist thermal simulation at 1000 s on a 512 × 256 grid. Left: perturbation potential temperature contoured every 0.5 K. Right: vertical velocity contoured every 2 m s<sup>-1</sup>, negative contours are dashed. Contrast to Fig. 3 in [3].

## 4.2 Comparison of Different Schemes

We now investigate the performance of the two-step split schemes detailed in section 33.2 for the moist thermal simulation. The **A-B** procedure –noted Split(I)– involves advancing the dynamics neglecting the phase transition terms,  $e_v$  in our case, during approximately  $\Delta t_{\text{sat}}$  before an adjustment step is performed to account for the saturation requirements. Alternatively, the **A\*-B** case –noted Split(II)– computes pressure with consistent values of temperature and water fractions, and thus updated moist thermodynamic properties, during the numerical integration of the dynamics. The reference solution is now given by the one-step coupled scheme that does not need to neglect  $e_v$  to compute the moist flow and assures the moist saturation requirements. In particular we evaluate the impact of  $\Delta t_{\text{sat}}$  on the numerical approximations.

### 4.2.1 Benchmark Problem

We consider again the moist configuration of the benchmark problem in [3], for which the previous results computed with the coupled scheme will be taken as the reference solutions. All simulations were carried out on a uniform grid of 256 × 128. Figure 5 compares results with the reference solution at 1000 s, for  $\Delta t_{\text{sat}} = 0$ , that is, an adjustment step is performed after each time integration step of the dynamics. In this particular case both approaches yield practically the same result taking into account that the numerical scheme used to solve system (20) is fully explicit in time; that is, system (20) is evolved in time starting from a state that satisfies the saturation requirements. However, for larger correction intervals ( $\Delta t_{\text{sat}} > 0$ ) the latter might not hold anymore.

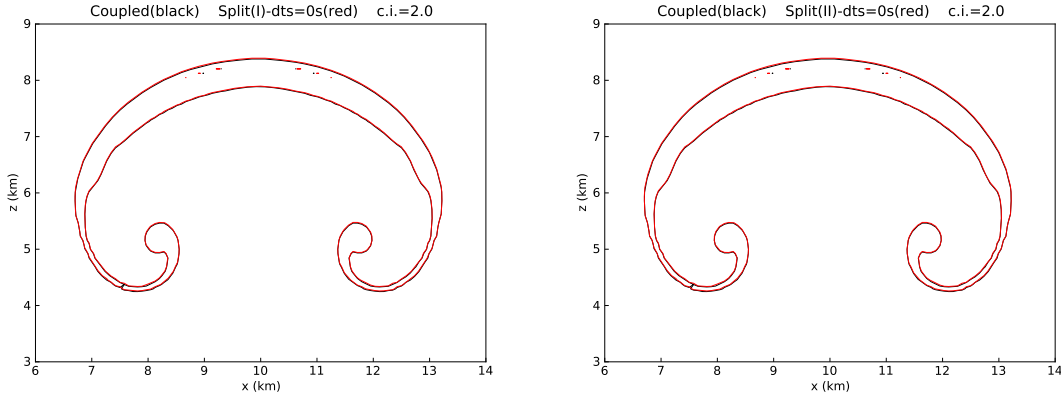


Figure 5: Split(I) (left) and Split(II) (right) solutions for  $\theta'_e$  with  $\Delta t_{\text{sat}} = 0$ , compared with the Coupled ones. Contours every 2 K.

If we now consider, for instance,  $\Delta t_{\text{sat}} = 3$  s, this is approximately equivalent to the time step considered in [20] to solve the same problem but in a pseudo-incompressible framework (specifically,  $\Delta t = 1.66$  s and  $\sigma^{\text{CFL}} = 0.5$  in [20]). It thus gives us an idea of the order of magnitude of the time steps needed to solve this particular problem without the influence of acoustic waves and consequently, of the corresponding time intervals that would be considered for the saturation adjustments. The goal of this illustration is then to mimic the case of slower adjustment paces ( $\Delta t_{\text{sat}}$ ) with respect to the acoustic time steps ( $\Delta t$ ) as a consequence of considering sound-proof equations (like in [20]) or because the  $\Delta t_{\text{sat}}$  corresponds to the time integration step of the slow modes (as in [3]), potentially larger than the time steps required to solve the acoustic modes disclosed by the compressible equations. We recall that in this study no numerical separation between slow and fast modes is performed and therefore the time integration steps  $\Delta t$  remains limited by the acoustic waves so that several  $\Delta t$  are required within each  $\Delta t_{\text{sat}}$ , as explained in § 33.2. Figure 6 illustrates the corresponding results for  $\Delta t_{\text{sat}} = 3$  s, and also for  $\Delta t_{\text{sat}} = 6$  s, for which the differences between both techniques become even more evident. It can thus be observed that fully neglecting moist thermodynamics associated in this case with phase changes during long intervals of time may cause important deviations from the reference moist dynamics and that some kind of coupling should be introduced in order to enhance the numerical approximations, as explained in § 33.2. With our formulation, in particular, computing pressure based on consistent values of temperature and water mass fractions during the time integration of the dynamics proves to be necessary for relatively large time steps in order to numerically capture the dynamics of the moist flow. However, using an iterative, nonlinear solver both during the time evolution of the dynamics and the adjustment step as in the Split(II) scheme certainly increases the computational costs. For this particular problem using the Split(II) procedure involves an overhead of about 10 to 15 % with respect to the coupled scheme. Finally, Figure 7 shows an extreme case with  $\Delta t_{\text{sat}} = 30$  s, for which it can be seen that the **A\*-B** solver still yields reasonably good approximations to the reference moist dynamics. As a comparison for  $\Delta t_{\text{sat}} = 0, 3, 6,$  and  $30$  s, the maximum vertical velocities obtained with the **A-B** solver are given by 13.3267, 12.9247, 12.6430, and 9.40192 m s<sup>-1</sup>, respectively; whereas the **A\*-B** solver yields 13.3266 m s<sup>-1</sup> in all cases.

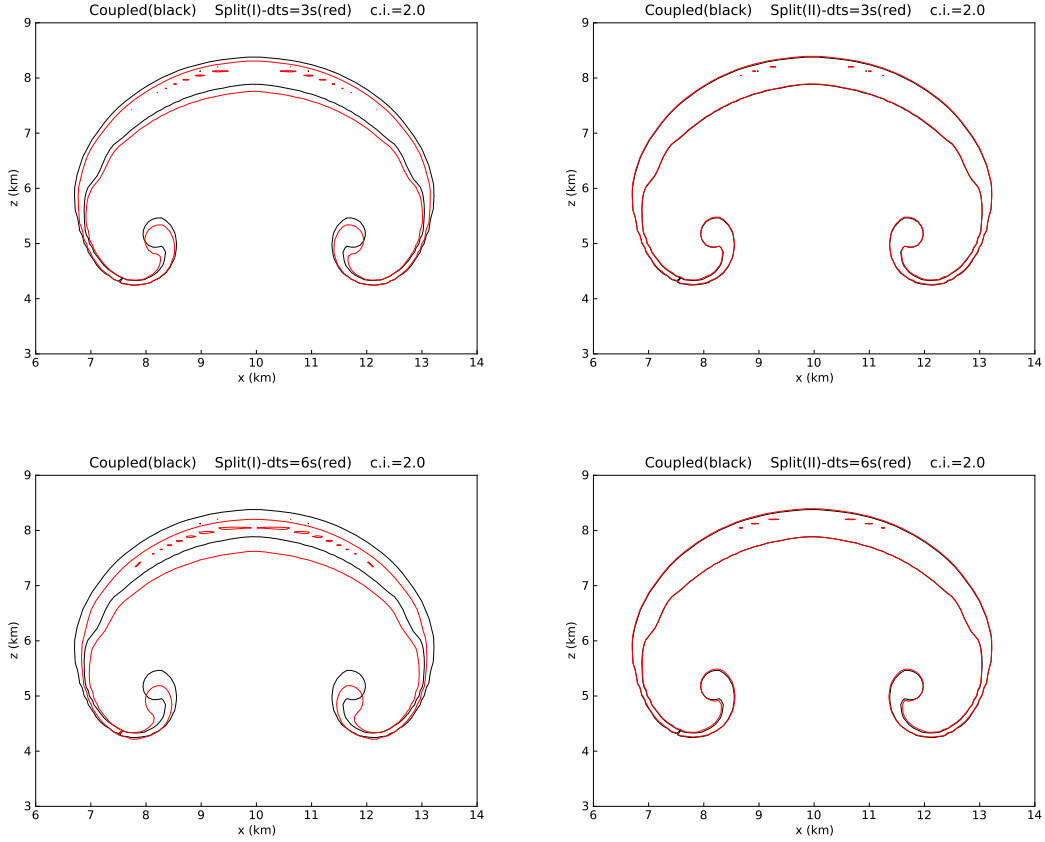


Figure 6: Split(I) (left) and Split(II) (right) solutions for  $\theta'_e$  with  $\Delta t_{\text{sat}} = 3 \text{ s}$  (top) and  $\Delta t_{\text{sat}} = 6 \text{ s}$  (bottom), compared with the Coupled ones. Contours every 2 K.

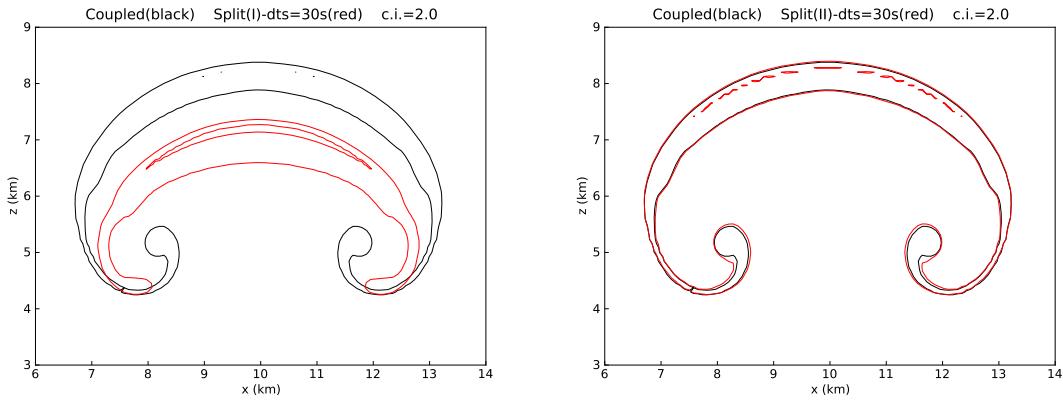


Figure 7: Split(I) (left) and Split(II) (right) solutions for  $\theta'_e$  with  $\Delta t_{\text{sat}} = 30 \text{ s}$ , compared with the Coupled ones. Contours every 2 K.

## 4.2.2 Non-isentropic Background State

We consider the hydrostatically balanced profiles in [5] (Eq. 2) for the background state:

$$\left. \begin{aligned} \theta_0(z) &= \theta_{00} \exp(Sz), \\ p_0(z) &= p_{00} \left[ 1 - \frac{g}{c_{pa}\theta_{00}S} (1 - \exp(-Sz)) \right]^{c_{pa}/R_a}, \end{aligned} \right\} \quad (28)$$

where  $\theta_{00}$  and  $p_{00}$  stand for the environmental potential temperature and pressure at the surface ( $z = 0$ ), with the static stability  $S$  defined as  $S = N^2/g = d \ln \theta_0 / dz$  ( $N$  is the Brunt-Väisälä frequency). The potential temperature is given by (22). For the following computations we define a computational domain 4 km high and wide, with periodic horizontal boundary conditions and the same vertical boundary conditions implemented for the previous benchmark problem. The same thermodynamic parameters from [3] are considered, whereas constants (13) coming from [23] are considered in the Clausius-Clapeyron equation (12) with  $p_{\text{trip}} = 611$  Pa. From [11], we take  $S = 1.3 \times 10^{-5} \text{ m}^{-1}$ ,  $\theta_{00} = 283$  K, and  $p_{00} = 850$  hPa. The stability of the dry background state can be thus measured by the squared Brunt-Väisälä frequency:  $N^2 \approx 1.3 \times 10^{-4} \text{ s}^{-2}$ . All simulations were performed on a uniform grid of  $256 \times 256$ .

For our formulation we also need to compute the hydrostatic base density  $\rho_0$  based on the background temperature and pressure (28), and the distribution of air, water vapor, and liquid water in the atmosphere. The latter quantities are set by the relative humidity in the atmosphere RH measured in percentage and defined as  $\text{RH} = (p_v/p_v^*) \times 100$ . In particular if  $\text{RH}_0 < 100\%$ , then no liquid water should be present in the atmosphere in order to guarantee the thermodynamic equilibrium of the initial state, that is,  $q_{l0}(z) = 0$ . We consider in this study two cases: first, a saturated medium, that is  $\text{RH}_0 = 100\%$  and  $r_t = 0.02$ , just like in the moist benchmark problem; and a second configuration with  $\text{RH}_0 = 20\%$ , and hence, no liquid water in the initial background state. Contrary to the benchmark configuration in [3], we have now in either case a non-isentropic background state, where the following definitions of specific entropy have been adopted according to [23]:

$$\begin{aligned} s_a &= c_{pa} \log \left( \frac{T}{T_{\text{trip}}} \right) - R_a \log \left( \frac{p}{p_{\text{trip}}} \right), \\ s_v &= c_{pv} \log \left( \frac{T}{T_{\text{trip}}} \right) - R_v \log \left( \frac{p}{p_{\text{trip}}} \right) + S_{0v}, \\ s_l &= c_{vl} \log \left( \frac{T}{T_{\text{trip}}} \right), \\ s_m &= q_a s_a + q_v s_v + q_l s_l, \end{aligned} \quad (29)$$

for dry air, water vapor, liquid water, and moist air, with  $S_{0v} = e_{0v}/T_{\text{trip}} + R_v$ .

Let us consider the first configuration with an initially saturated environment. In this case the moist squared Brunt-Väisälä frequency  $N_m^2$  can be computed according to [7] (eqs. 36–37), which yields a stable stratification for  $N_m^2$  monotonically varying from  $3.5 \times 10^{-6} \text{ s}^{-2}$  at the surface up to  $1.3 \times 10^{-5} \text{ s}^{-2}$  at the top of the computational domain. Similar to (25), we introduce a warm perturbation on temperature:

$$T' = 2 \cos^2 \left( \frac{\pi L}{2} \right), \quad (30)$$

where  $L$  is defined by (26), with  $x_c = 2$  km,  $z_c = 0.8$  km, and  $x_r = z_r = 300$  m. The water distributions, as well as the density, are thus adjusted to the perturbed temperature with the original pressure field. As for the previous problem both the coupled and the split schemes with

$\Delta t_{\text{sat}} = 0$ , yield practically the same solutions, with  $\sigma^{\text{CFL}} = 0.9$  and roughly constant time steps of about 0.04 s. Increasing the interval  $\Delta t_{\text{sat}}$  to adjust moist variables to saturation requirements has the same effect as previously noticed for the benchmark problem with isentropic static base. Figure 8 illustrates the latter behavior in terms of the specific entropy of moist air (eq. (29)) for  $\Delta t_{\text{sat}} = 0.6$  and 6 s, after 300 s of integration. Simulations were stopped before the nonlinearities become more apparent and sub-grid turbulence starts playing a more important role in the dynamics, as analyzed in [11]. We recall that for the sake of simplicity sub-grid turbulence is not considered in the present study. The interval of 0.6 s for  $\Delta t_{\text{sat}}$  takes into account the same ratio considered for the benchmark problem (about 15 with respect to the compressible time stepping), just to have an approximate idea of the size of time steps required without the influence of acoustic modes, either numerically or analytically circumvented.

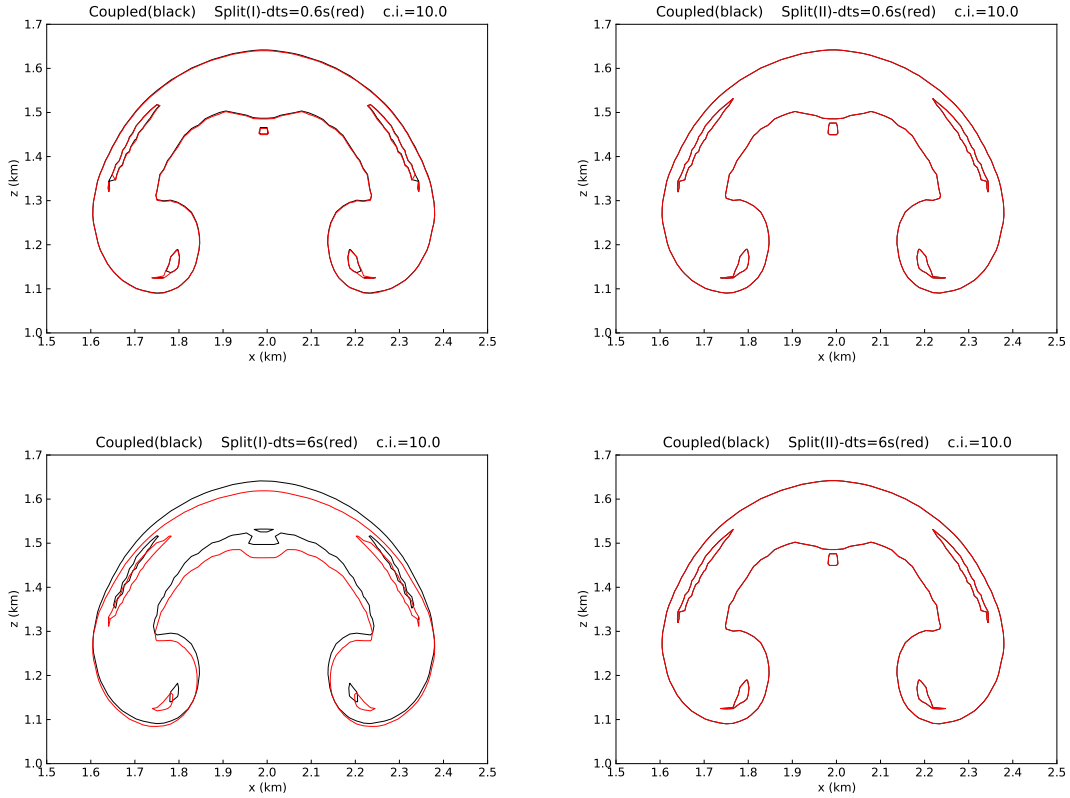


Figure 8: Initially saturated, non-isentropic background state. Split(I) (left) and Split(II) (right) solutions for  $s_m$  after 300 s with  $\Delta t_{\text{sat}} = 0.6$  s (top) and  $\Delta t_{\text{sat}} = 6$  s (bottom), compared with the Coupled ones. Contours every  $10 \text{ J kg}^{-1} \text{ K}^{-1}$ .

For the second configuration with  $\text{RH}_0 = 20\%$ , we consider the same temperature perturbation (30) and an additional circular perturbation on the relative humidity, which is set to 100% for a radius  $r < 200$  m, as considered in [11]. A transition layer is assumed such that

$$\text{RH} = \text{RH}_0 + (100 - \text{RH}_0) \cos^2\left(\frac{\pi}{2} \frac{r - 200}{100}\right), \quad 200 \leq r \leq 300, \quad (31)$$

taken also from [11]. Initially there is no liquid water in the domain, not even in the saturated region, whereas the perturbed water vapor is recomputed based on (30) and (31) with the original

static pressure. After performing the same tests with the different numerical techniques, the same observations can be made in terms of moist saturation adjustments. For larger intervals  $\Delta t_{\text{sat}}$ , a stronger coupling needs to be taken into account between the solution of the dynamics and moist processes in order to guarantee a reasonably accurate reproduction of the global phenomenon in accordance to the reference moist flow. Figure 9 illustrates the latter with an adjustment interval of  $\Delta t_{\text{sat}} = 6$  s; once again  $\sigma^{\text{CFL}} = 0.9$ , which yields roughly constant time steps of about 0.04 s. Notice that in this case, differences between the split and coupled approximations are smaller with respect to the previous configurations for saturated and both isentropic and non-isentropic environments. This is due to the fact that all the liquid water is mainly contained in the perturbed area and hence only this region is subjected to phase changes and active moist microphysics.

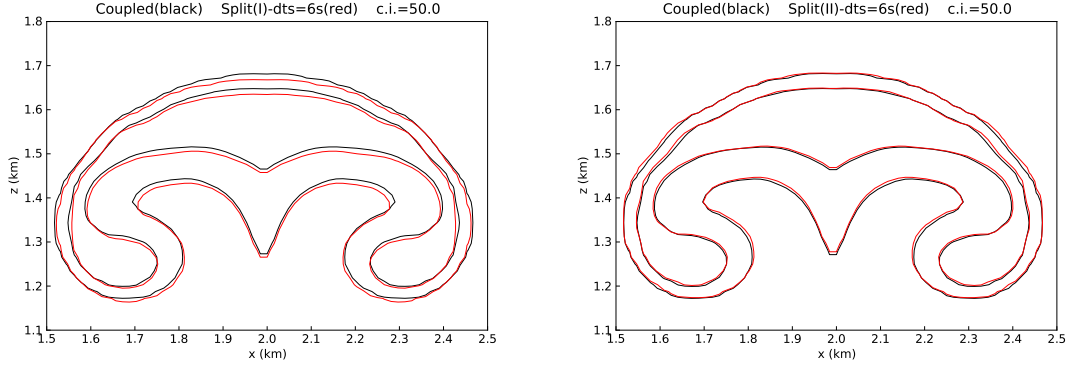


Figure 9: Non-isentropic background state with a partially saturated perturbation. Split(I) (left) and Split(II) (right) solutions for  $s_m$  after 300 s with  $\Delta t_{\text{sat}} = 6$  s (bottom) compared with the Coupled ones. Contours every  $50 \text{ J kg}^{-1} \text{ K}^{-1}$ .

## 5 Summary

In this paper we have studied the incorporation of reversible moist processes, namely phase change phenomena and moist thermodynamic properties, in atmospheric flows. For the purpose of this study, the dynamics were explicitly evolved at the acoustic time scale, based on the compressible Euler equations, with conservation equations for total density of moist air, momentum, and energy of moist air. Two approaches were implemented with this formulation. In the first case a one-step, coupled procedure solves simultaneously the equations of motion together with the conservation equation for total water content. Because of the choice of variables, in particular because the energy of moist air includes the contribution of both sensible and latent heats, this formulation does not include source terms related to phase change in either the energy or the moist variable equations, and therefore the system of equations can be solved without the need to either estimate or neglect the latter source terms. Pressure is computed through the moist equation of state for which temperature and moist variables in terms of water vapor and liquid water must be diagnostically recovered using the saturation requirements. In the second approach source terms related to phase change appear, but only in the equations for water vapor and liquid water mass fractions. A two-step technique is then implemented in which the the dynamics are first evolved together with the conservation equations for water vapor and liquid water in which source terms related to phase change have been neglected. Since vapor and liquid water contents are available with this formulation, pressure can be directly computed using the moist equation of state. In a second step moist variables are adjusted according to a time interval  $\Delta t_{\text{sat}}$  such that the saturation requirements are satisfied. Notice that

this two-step procedure differs from other similar applications (like the ones in [3, 25]) in that phase change related terms are present only in the equation for moist variables and thus the equations of motion (written in terms of density, momentum, and energy) remain unchanged for both the one- and the two-step procedures.

A well-established benchmark problem introduced in [3] was then studied to validate the numerical techniques described. In this way we could define a reference solution that describes the moist flow without neglecting any moist thermodynamic mechanism during the numerical integration (the Coupled solution) and evaluate the two-step approximation (the Split(I) solution). With time steps for the dynamics sufficiently small to resolve the fast acoustic modes, we investigated the impact of incorporating moist reversible processes on a slower time scale. Numerical tests showed that such a scale gap between dynamics and moist saturation adjustments may lead to serious deviations from the reference coupled dynamics and that variations in moist thermodynamic properties should be consistently taken into account during the numerical integration of the dynamics. The latter is achieved with our formulation by computing pressure based on saturation requirements for moist variables and temperature (the Split(II) solution). Further testing with both isentropic and non-isentropic background states, as well as saturated and non-saturated initial configurations, confirmed the initial findings. It is hoped that the insight gained here as to how strongly the moist processes should be numerically coupled to the dynamics will carry over from dynamical evolution on the acoustic time scale to the more realistic, and computationally efficient, evolution on the advective time scale. This will be further investigated and discussed in future work.

## Acknowledgements

The work in the Center for Computational Sciences and Engineering at LBNL was supported by the Applied Mathematics Program of the DOE Office of Advance Scientific Computing Research under U.S. Department of Energy under contract No. DE-AC02-05CH11231. DR was supported by the Scientific Discovery through Advanced Computing (SciDAC) program funded by U.S. Department of Energy Office of Advanced Scientific Computing Research and Office of Biological and Environmental Research.

## References

- [1] A. S. Almgren, V. E. Beckner, J. B. Bell, M. S. Day, L. H. Howell, C. C. Joggerst, M. J. Lijewski, A. Nonaka, M. Singer, and M. Zingale. CASTRO: A new compressible astrophysical solver. I. Hydrodynamics and self-gravity. *ApJ*, 715:1221–1238, 2010.
- [2] G. K. Batchelor. The conditions for dynamical similarity of motions of a frictionless perfect-gas atmosphere. *Q. J. Roy. Meteor. Soc.*, 79:224–235, 1953.
- [3] G. H. Bryan and J. M. Fritsch. A benchmark simulation for moist nonhydrostatic numerical models. *Mon. Wea. Rev.*, 130:2917–2928, 2002.
- [4] T.L. Clark. A small-scale dynamic model using a terrain-following coordinate transformation. *J. Comput. Phys.*, 24:186–215, 1977.
- [5] T.L. Clark and R.D. Farley. Severe downslope windstorm calculations in two and three spatial dimensions using anelastic interactive grid nesting: A possible mechanism for gustiness. *J. Atmos. Sci.*, 41:329–350, 1984.
- [6] D. R. Durran. Improving the anelastic approximation. *J. Atmos. Sci.*, 46(11):1453–1461, 1989.
- [7] D.R. Durran and J.B. Klemp. On the effects of moisture on the Brunt-Väisälä frequency. *J. Atmos. Sci.*, 39:2152–2158, 1982.

- [8] J. A. Dutton and G. H. Fichtl. Approximate equations of motion for gases and liquids. *J. Atmos. Sci.*, 26:241–254, 1969.
- [9] K. A. Emanuel. *Atmospheric Convection*. Oxford University Press, 1994.
- [10] D. O. Gough. The anelastic approximation for thermal convection. *J. Atmos. Sci.*, 26:448–456, 1969.
- [11] W.W. Grabowski and T.L. Clark. Cloud-environment interface instability: Rising thermal calculations in two spatial dimensions. *J. Atmos. Sci.*, 48:527–546, 1991.
- [12] W.W. Grabowski and P.K. Smolarkiewicz. Monotone finite-difference approximations to the advection-condensation problem. *Mon. Weather Rev.*, 118:2082–2097, 1990.
- [13] W.W. Grabowski and P.K. Smolarkiewicz. A multiscale anelastic model for meteorological research. *Mon. Weather Rev.*, 130:939–956, 2002.
- [14] T. Hauf and H. Höller. Entropy and potential temperature. *J. Atmos. Sci.*, 44:2887–2901, 1989.
- [15] J. B. Klemp and R. B. Wilhelmson. The simulation of three-dimensional convective storm dynamics. *J. Atmos. Sci.*, 35:1070–1096, 1978.
- [16] J.B. Klemp, W.C. Skamarock, and J. Dudhia. Conservative split-explicit time integration methods for the compressible nonhydrostatic equations. *Mon. Wea. Rev.*, 135:2897–2913, 2007.
- [17] M.J. Kurowski, W.W. Grabowski, and P.K. Smolarkiewicz. Towards multiscale simulation of moist flows with soundproof equations. *J. Atmos. Sci.*, 70:3995–4011, 2013.
- [18] F. Lipps and R. Hemler. A scale analysis of deep moist convection and some related numerical calculations. *J. Atmos. Sci.*, 39:2192–2210, 1982.
- [19] Y. Ogura and N. A. Phillips. Scale analysis of deep and shallow convection in the atmosphere. *J. Atmos. Sci.*, 19:173–179, 1962.
- [20] W. P. O’Neill and R. Klein. A moist pseudo-incompressible model. *Atmos. Res.*, 2013.
- [21] K.V. Ooyama. A thermodynamic foundation for modeling the moist atmosphere. *J. Atmos. Sci.*, 47:2580–2593, 1990.
- [22] K.V. Ooyama. A dynamic and thermodynamic foundation for modeling the moist atmosphere with parameterized microphysics. *J. Atmos. Sci.*, 58:2073–2102, 2001.
- [23] D. M. Romps. The dry-entropy budget of a moist atmosphere. *J. Atmos. Sci.*, 65:3779–3799, 2008.
- [24] M. Satoh. Conservative scheme for the compressible nonhydrostatic models with the horizontally explicit and vertically implicit time integration scheme. *Mon. Wea. Rev.*, 130:1227–1245, 2002.
- [25] M. Satoh. Conservative scheme for a compressible nonhydrostatic model with moist processes. *Mon. Wea. Rev.*, 131:1033–1050, 2003.
- [26] M. Satoh, T. Matsuno, H. Tomita, H. Miura, T. Nasuno, and S. Iga. Nonhydrostatic icosahedral atmospheric model (NICAM) for global cloud resolving simulations. *J. Comput. Phys.*, 227:3486–3514, 2008.
- [27] S.-T. Soong and Y. Ogura. A comparison between axisymmetric and slab-symmetric cumulus cloud models. *J. Atmos. Sci.*, 30:879–893, 1973.

- [28] M.C. Tapp and P.W. White. A non-hydrostatic mesoscale model. *Q. J. Roy. Meteor. Soc.*, 102(432):277–296, 1976.
- [29] L. J. Wicker and W. C. Skamarock. A time-splitting scheme for the elastic equations incorporating second-order Runge–Kutta time differencing. *Mon. Wea. Rev.*, 126:1992–1999, 1998.